Targeted medication delivery using magnetic nanostructures

2007 J. Phys.: Condens. Matter 19 086210

(http://iopscience.iop.org/0953-8984/19/8/086210)

IOP PUBLISHING JOURNAL OF PHYSICS: CONDENSED MATTER

J. Phys.: Condens. Matter **19** (2007) 086210 (9pp) doi:10.1088/0953-8984/19/8/086210

Targeted medication delivery using magnetic nanostructures

Mina Yoon[1,2], **Peter Borrmann**[3] **and David Tománek**[4,5]

[1] Materials Science and Technology Division, Oak Ridge National Laboratory, Oak Ridge, TN 37831-6032, USA
[2] Department of Physics and Astronomy, The University of Tennessee, Knoxville, TN 37996, USA
[3] Physics Department, University Oldenburg, 26111 Oldenburg, Germany
[4] Physics and Astronomy Department, Michigan State University, East Lansing, MI 48824-2320, USA
[5] Institute for Theoretical Physics, University of Regensburg, 93040 Regensburg, Germany

Received 8 November 2006
Published 9 February 2007
Online at stacks.iop.org/JPhysCM/19/086210

Abstract

We use quaternion molecular dynamics simulations to describe field-induced structural transitions in systems of few magnetic dipoles and their use for targeted medication delivery. Compact ring isomers of magnetic particles are contained, together with molecules of an active medication, inside inert microcapsules. The filled microcapsules may be transported within the body using a weak, inhomogeneous magnetic field. Medication release is triggered by puncturing the container during a structural transition within the magnetic subsystem, induced by an externally applied strong magnetic field. Our simulations describe not only the time evolution of the magnetic subsystem during a successful medication release, but also address ways to suppress an accidental release induced by thermal and magnetic fluctuations.

(Some figures in this article are in colour only in the electronic version)

1. Introduction

Finite aggregates of small magnetic particles, such as those found in ferrofluids [1–4], are intriguing systems with a wide range of technological applications [5]. The magnetic particles, mostly consisting of magnetite, have a typical diameter of tens of nanometres, carry a large permanent magnetic moment of the order of 10^4–10^5 μ_B, and are covered by an approximately 2 nm thick surfactant layer, which prevents their coalescence in a viscous suspension at room temperature. In large systems, spontaneous formation of complex labyrinthine [6, 7] and branched [3] structures has been observed and theoretically addressed [1, 2, 8–15] at low temperatures and in applied magnetic fields. Of particular interest in this study is the fact that, due to the dominant dipole–dipole interparticle interaction, aggregates of $4 \lesssim n \lesssim 14$

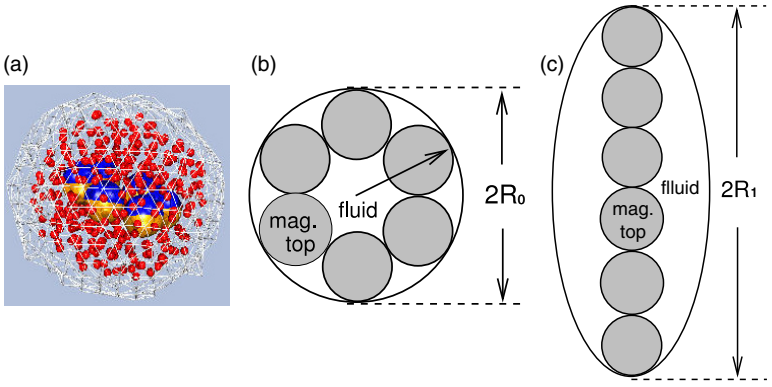

Figure 1. Schematic diagram of the magnetic medication delivery mechanism. (a) Typical structure of a microcapsule, containing six magnetic tops and 'medication', in zero field. The enclosing membrane, shown in white, is represented by a 368 particle mesh. The 375 medication particles are shown by small spheres. The magnetic tops are represented by the large spheres, with the dark hemisphere indicating their north and the light hemispheres their south pole. (b) In zero field, the equilibrium structure of the tops is a ring that fits into a spherical membrane container of radius R_0. (c) In a strong magnetic field, the ring transforms to a chain, thus deforming the container to an ellipsoid with the long axis R_1. For a container with finite tensile strength, the capsule bursts if $R_1 \gg R_0$.

magnetic tops are a classically tunable two-level system [16]. The most stable structure of such finite-size dipole systems is a ring in zero field and a chain in large external magnetic fields [4].

In this contribution, we describe a possible application of such magnetic nanostructures for targeted medication delivery. We will consider the behaviour of inert microcapsules that contain a small number of magnetic particles along with an active medication, shown in figure 1(a). The filled microcapsules may be transported within the body using a weak, inhomogeneous magnetic field. Once concentrated in a target area, a structural transition in the magnetic subsystem from a ring, shown in figure 1(b), to a chain, depicted in figure 1(c), is triggered by an external magnetic field [4]. This causes the microcapsules to burst, thus releasing the encapsulated medication.

Microcapsules have been used extensively in medicine as micro-containers that transport and deliver an active substance to a specific site in the human body. Their typical diameter of 0.1 μm is small enough to allow the microcapsules to pass through all capillary blood vessels. A very attractive application of this technique appears to be in the chemotherapy of cancer, since the most potent drugs are indiscriminately toxic to all tissue. These drugs should preferably be delivered only in the tumour region to limit the damage to healthy tissue and the total toxic load on the body.

To regulate medication delivery, it has been common practice to encapsulate the active medication in membranes formed of albumin, polyalkylcyanoacrylate, ethylcellulose or polyglutaraldehyde, which dissolve spontaneously over the course of time. Here we describe an alternate local medication delivery mechanism, based on the structural transition occurring in aggregates of magnetic tops. This transition, which releases the medication in a planned fashion [17], is triggered by applying a magnetic field.

There is significant freedom in optimizing this system for the delivery of particular medications, including changing the microcapsule diameter, the tensile strength of the membrane, the size and magnetic moment of the tops, the spatial variation, the strength, and the time dependence of the externally applied magnetic field. These system variables should be

optimized to ensure planned delivery, and also to avoid accidental delivery due to thermal and magnetic fluctuations, as well as other environmental variables.

2. Computational approach

We consider a microcapsule containing N spherical magnetic tops and N_{m} particles representing the active medication, contained in a flexible membrane, represented by a mesh of N_c particles, as shown in figure 1(a). The key component of the delivery mechanism is the magnetic particles carrying a large permanent magnetic moment μ_0, which undergo a structural transition in a strong magnetic field.

In a system of magnetic tops in an external magnetic field $\boldsymbol{H}$, the potential energy U_{tot} contains the interaction of each dipole[6] $\mu_0\hat{\boldsymbol{\mu}}$ with the field and pairwise interactions, given by

$$U_{\mathrm{tot}} = -\mu_0 \sum_i \hat{\boldsymbol{\mu}}_i \cdot \boldsymbol{H} + \sum_{j>i} \left(u_{ij}^{dd} + u_{ij}^{nm}\right). \tag{1}$$

The magnetic interaction u_{ij}^{dd} between two identical dipoles, separated by $\boldsymbol{r}_{ij} = \boldsymbol{r}_j - \boldsymbol{r}_i$, has the classical form [19]

$$u_{ij}^{dd} = (\mu_0^2/r_{ij}^3)\left[\hat{\boldsymbol{\mu}}_i \cdot \hat{\boldsymbol{\mu}}_j - 3(\hat{\boldsymbol{\mu}}_i \cdot \hat{\boldsymbol{r}}_{ij})(\hat{\boldsymbol{\mu}}_j \cdot \hat{\boldsymbol{r}}_{ij})\right]. \tag{2}$$

To prevent a spontaneous collapse of the magnetic nanostructures, we augment the dipole–dipole interactions by an isotropic non-magnetic interparticle interaction u_{ij}^{nm} with a soft-core short-range repulsion, caused by the entropic repulsion between surfactant layers, and a long-range attraction, which can be associated with van der Waals interaction. To accelerate convergence, we describe the attractive and repulsive terms by exponential functions, as

$$u_{ij}^{nm} = \left[\epsilon_1 \left(\frac{\sigma}{r_{ij}}\right)^{p_1} \exp\left(\frac{\sigma - r_{ij}}{\rho_1}\right) - \epsilon_2 \left(\frac{\sigma}{r_{ij}}\right)^{p_2} \exp\left(\frac{\sigma - r_{ij}}{\rho_2}\right)\right]. \tag{3}$$

To obtain the total energy, the potential energy has to be augmented by the translational and rotational kinetic energy of the tops as

$$E = U_{\mathrm{tot}} + \sum_i \tfrac{1}{2} m_i v_i^2 + \sum_i \tfrac{1}{2} I_i {\omega_i}^2, \tag{4}$$

where m_i is the mass, v_i the velocity, I_i the inertia, and ω_i the angular velocity of particle i.

In realistic simulations representing medication delivery, the particles representing the medication and the enclosing membrane also have to be considered explicitly. In this complete system, the sums in equations (1) and (4) extend also over the membrane and medication particles. These particles are non-magnetic, have vanishing inertia, and their isotropic mutual interaction may be described by equation (3).

Our simplistic approach for interparticle interactions needs to be justified in particular for the membrane. Even though more sophisticated descriptions of membranes exist [18], they are not crucial for reproducing our magnetically driven medication delivery method. Since it is only the finite tensile strength of the membrane that is important for the delivery mechanism we discuss, we model the membrane in the simplest possible way as a mesh of particles interacting with a finite-depth pairwise potential.

3. Results and discussion

As medication delivery is triggered by a field-induced ring-to-chain transition, we first need to ensure that the ring structure remains intact if the system is subject to thermal and magnetic fluctuations, thus preventing accidental medication delivery. On the other hand, we need

[6] We define $\hat{x} = \boldsymbol{x}/x$ as the directional unit vector.

to understand the conditions resulting in forming a chain [20], and thus ensure the planned medication delivery in spite of possible thermal and magnetic fluctuations [4, 16, 17].

To achieve this, we first performed quaternion molecular dynamics (QMD) simulations of six magnetic dipoles confined in a spherical cavity at different fields and temperatures, ignoring the presence of medication particles and possible container deformations. We used quaternion coordinates [21] to properly describe the rotational motion of the magnetic tops and to avoid divergencies in solving the rotational equations of motion. The magnetic tops of magnetite have a diameter $\sigma = 20$ nm, mass $m = 13.12 \times 10^6$ amu, inertia $I = 5.248 \times 10^{10}$ amu Å^{-2}, and carry a large permanent magnetic moment $\mu_0 = 1.68 \times 10^5\ \mu_B$. We treated the system as a microcanonical ensemble and monitored its behaviour during a gradual, stepwise heating process. In a microcanonical ensemble, we interpreted the averaged kinetic energy of the system as an effective temperature T. Temerature changes were achieved by rescaling the velocities, followed by an equilibration time.

We chose the equilibrium geometry of the magnetic dipoles in a given magnetic field as the starting configuration in our QMD simulations. To mimic the effect of the container membrane, we confined the system in a rigid spherical cavity with a 80 nm radius and a soft surface[7]. We used a time step of 0.01 ns and integrated the Euler–Lagrange equations of motion using a fourth-order Runge–Kutta algorithm to determine the particle trajectories [22]. After changing the effective temperature by rescaling the velocities, the system was first allowed to equilibrate during 10^6 time steps, corresponding to 10.0 μs, before data were collected.

For small systems of 4–14 magnetic dipoles, the equilibrium geometry at $T = 0$ is known to change from a perfect ring in zero field to a chain in high magnetic fields [4]. Since the dipole–dipole interaction is significant in comparison to $k_B T$ even at room temperature, the ring structure is predominant in zero field even at $T = 300$ K, as seen in figure 2(b). Similarly, the chain structure prevails in an applied field $H = 1500$ Oe at $T = 300$ K, as seen in figure 3(b).

The calculated thermodynamic behaviour of the system as a function of the effective temperature is shown in figure 2(a) for zero applied field and in figure 3(a) for the field $H = 1500$ Oe. We present averages of different observables, obtained during 10^6 time steps each, with the error bars reflecting fluctuations in this finite system.

The total energy per particle, E/N, is displayed in the left panels of figures 2(a) and 3(a) as the basic thermodynamic quantity, which indicates the onset of phase transitions and their counterparts in finite-size systems. Since we are focusing on the ring-to-chain transition in systems of magnetic dipoles, we found it useful to monitor the ratio between the total and the maximum magnetic moment of the system, μ_{tot}/μ_{max}, where $\mu_{max} = N\mu_0$. Since $\mu_{tot}/\mu_{max} \approx 0$ for ring structures and $\mu_{tot}/\mu_{max} \approx 1$ for chains, we find this quantity a good indicator of structural changes, and display it in the middle panels of figures 2(a) and 3(a). Unfortunately, we also expect a large value of μ_{tot}/μ_{max} in fragmented structures including systems of isolated dipoles, which align individually with the field. As an indicator of fragmentation in the system, we introduce the average closest interparticle distance, defined as $D_{nn} = (1/N)\sum_i \min\{r_{ij}\}$, and display its temperature dependence in the right panels of figures 2(a) and 3(a). In the summation over all particles i, the minimum is taken over its distance r_{ij} from all the other particles j in the system. We thus expect $D_{nn} \approx \sigma$ for a contiguous system, and can interpret an increase in D_{nn} as an indication that individual magnetic tops have fragmented off.

In the case of zero applied magnetic field, addressed in figure 2(a), we observe a gradual increase of the energy per particle E/N with temperature. For $T \gtrsim 800$ K and $T \lesssim 300$ K,

[7] The potential used to confine the magnetic particles in a rigid, spherical cavity is given by $V(r) = \epsilon \exp[(r - r_0)/\sigma]$, with $\sigma = 0.1$ nm, $\epsilon = 1.0$ eV, and $r_0 = 80.0$ nm.

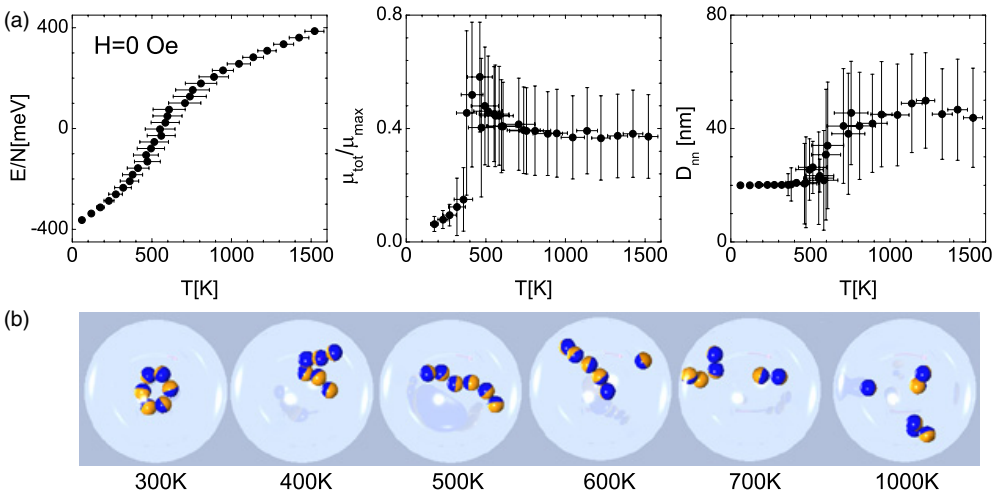

Figure 2. Thermodynamic behaviour of a finite system of magnetic dipoles, contained in a rigid spherical cavity with a 80 nm radius, in zero external field. (a) Results of microcanonical quaternion molecular dynamics simulations for a system of six magnetic dipoles. The left panel shows the energy per particle E/N as a function of the kinetic temperature T of the system, which is controlled by the total energy. The temperature gradient of the energy has a nearly constant classical value of the specific heat below 300 K and above 800 K. The change in the gradient occurring between these temperatures, generally indicative of a phase transition, is gradual due to the finite number of particles. The middle panel displays the ratio between the time-averaged total magnetic moment $\mu_{\rm tot}$ and the maximum magnetic moment $\mu_{\rm max}$ as a function of temperature, as an indicator of ring-to-chain transitions in contiguous structures. The right panel displays the temperature dependence of the average closest interparticle separation $D_{\rm nn}$, an indicator of particle evaporation. (b) Snapshots of typical structures observed at $T \approx 300$, 400, 500, 600, 700, and 1000 K.

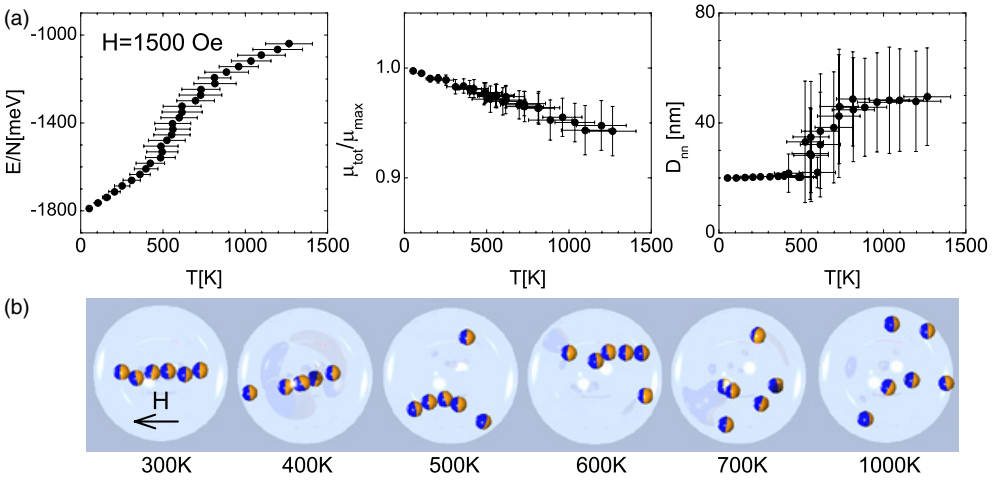

Figure 3. Thermodynamic behaviour of a finite system of magnetic dipoles, contained in a rigid spherical cavity with a 80 nm radius, in an external field $H = 1500$ Oe, with results presented in analogy to figure 2. (a) Energy E, magnetic moment μ, and closest interparticle separation $D_{\rm nn}$ obtained during microcanonical molecular dynamics simulations for a system of six magnetic dipoles. (b) Geometry snapshots at $T \approx 300$, 400, 500, 600, 700, and 1000 K.

the temperature gradient of the energy, representing the specific heat, behaves as expected for interacting (low temperatures) and for free (high temperatures) particles with six degrees of freedom per particle. A gradual, local increase in the specific heat, observed in the temperature range 300 K $\lesssim T \lesssim$ 800 K, is the finite-size counterpart of a first-order phase transition [16] from a ring to a chain and eventually to a gas of isolated dipoles, as seen in the structural snapshots depicted in figure 2(b). This transition temperature agrees within an order of magnitude with an estimate based on comparing the energy difference between a chain and a ring, 33 meV per particle, to $k_{\mathrm{B}}T$. The enthalpy associated with this transition also agrees well with the energy investment of 456 meV needed to break a nearest-neighbour bond in a chain.

As discussed above, an increase in the quantity $\mu_{\mathrm{tot}}/\mu_{\mathrm{max}}$ is a good indicator of a ring-to-chain transition in contiguous structures. Our results, shown in the middle panel of figure 2(a), are consistent with an abrupt ring-to-chain transition at $T \approx 350$ K. We consider this transition a counterpart of the melting transition at T_{m}, which preserves the short-range order, but changes the long-range order. As seen in the $T = 400$ and 500 K snapshots in figure 2(b), the chain is not straight above the transition, thus reducing the total magnetic moment to $\mu_{\mathrm{tot}}/\mu_{\mathrm{max}} < 1$. The system of dipoles is still contiguous at these temperatures, as suggested by a near-constant value of $D_{\mathrm{nn}}(T) \approx \sigma$ for $T \lesssim 500$ K in the right panel of figure 2(a). Further inspection of $D_{\mathrm{nn}}(T)$ suggests the onset of fragmentation near 500–700 K, which we associate with the boiling point T_{b}. Above this temperature, D_{nn} maintains a finite value, limited by the size of the enclosing cavity.

In the case of a large applied magnetic field $H = 1500$ Oe, addressed in figure 3(a), we deal with a chain structure, as suggested by the temperature dependence of $\mu_{\mathrm{tot}}/\mu_{\mathrm{max}}$ and the series of snapshots in figure 3(b). Even though there is no ring-to-chain transition, the energy per particle displays a similar temperature dependence as that in zero field, depicted in figure 2(a). To understand this behaviour, we compare the temperature dependence of the closest-particle distance D_{nn} in the absence and in the presence of an applied field in the right panels of figures 2(a) and 3(a). In both cases, we observe an increase of the observable $D_{\mathrm{nn}}(T) \approx \sigma$ above $T \approx$ 500–700 K, which we consider to be the finite-size counterpart of the boiling point. The fragmentation of the system in this temperature range is clearly reflected in figure 3(b). Considering the magnitude of the applied field $H = 1500$ Oe, the dipole–dipole interaction is almost one order of magnitude weaker than the interaction of individual dipoles with the field, about 1.5 eV in magnitude. Comparing this energy to temperature fluctuations, we expect $\mu_{\mathrm{tot}}/\mu_{\mathrm{max}}$ to decrease at a near-constant rate of -5.89×10^{-5} K^{-1} in the temperature range considered here, which compares well with the data displayed in the middle panel of figure 3(a).

The above results confirm that no structural transitions in the magnetic subsystem should occur below 350 K, ensuring no accidental rupture of the container membrane, thus preventing accidental medication delivery outside the targeted area in a live patient. On the other hand, transition to a chain, causing rupturing of the container membrane and thus a planned medication delivery, is ensured at 300 K under the influence of an applied field of 1500 Oe.

Fulfilling these two prerequisites for a safe application of our system to deliver medication, we performed a second set of QMD simulations, this time studying the dynamics of the complete microcapsule following its exposure to a relatively strong[8] static external field of 1500 Oe.

Even though the structural transitions we study here are quite general in nature and rather independent of the system size, we present results for a particular 'realistic' system, consisting

[8] Available clinical studies indicate that magnetic fields up to 2×10^4 Oe, which are commonly used in magnetic resonance imaging (MRI), are not directly harmful to humans. See [23].

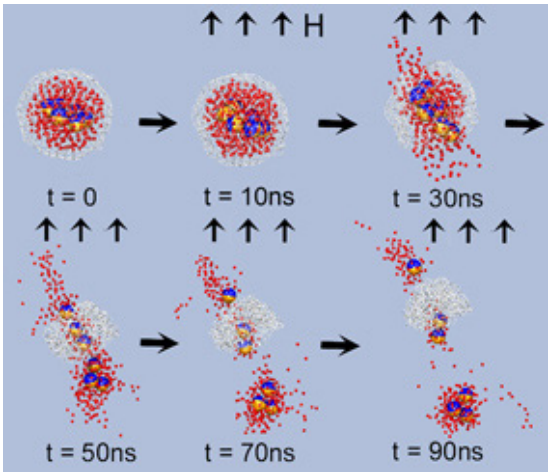

Figure 4. Time evolution of the microcapsule, after its initial equilibration at $T = 300$ K in zero field. A uniform field $H = 1500$ Oe is switched on at time $t = 0$. The five structural snapshots at $t = 10$, 30, 50, 70, and 90 ns display the response of the system to the applied field. As in figure 1(a), the large spheres represent the magnetic particles, with the dark hemisphere indicating their north and the light hemisphere their south pole. Field-induced structural rearrangement of the magnetic tops ruptures the container membrane, represented by the white mesh, thus causing the release of the active medication, represented by the small dark spheres. The direction of the applied field H is indicated by arrows.

Table 1. Parameters describing the isotropic interparticle interactions in equation (3). F denotes the ferromagnetic particles, M the medication, and C particles forming the container.

Particle pair	ϵ_1 (meV)	ϵ_2 (meV)	σ (nm)	ρ_1 (nm)	ρ_2 (nm)	p_1	p_2
F–F	64.0	64.0	20.00	0.50	1.00	4	0
M–M	64.0	64.0	9.30	0.50	1.00	4	0
C–C	900.0	900.0	9.30	0.70	1.40	1	0
F–M	200.0	200.0	14.00	0.59	1.18	1	0
F–C	226.0	226.0	14.00	0.59	1.18	1	0
M–C	800.0	0.0	8.00	0.70	1.40	1	0

of 375 medication particles and six spherical magnetic tops, contained in a triangular mesh membrane of 368 particles. The medication particles of mass $m = 0.15\times10^6$ amu and the membrane particles of mass $m = 0.3\times10^6$ amu are considered to be point-like, with no inertia. They are non-magnetic, and their mutual interactions are described by equation (3), with interaction parameters summarized in table 1. The near-spherical shape of the cage, seen in figures 1(a) and 4, results from the internal pressure, caused by the repulsion between the enclosed particles.

In contrast to the previous studies, we considered the complete microcapsule system as a canonical ensemble, coupled to a Nosé–Hoover thermostat [24, 25], which maintains its temperature at $T = 300$ K. We used the time step of 0.01 ns when integrating the equations of motion using a fourth-order Runge–Kutta algorithm. After the initial equilibration in zero field, we switched on a uniform field $H = 1500$ Oe at the time $t = 0$ and followed the time evolution of the system during the next 100 ns.

The results of our simulation[9] are shown as consecutive snapshots in figure 4. Up to about 20 ns after the onset of the magnetic field, the magnetic particles maintain their ring configuration. To minimize its energy, the ring rotates rigidly and aligns its normal with the field, with no effect on the container membrane. About 20 ns after switching on the magnetic field, the magnetic particles undergo a large change to a chain-like structure, which disrupts the container membrane and thus releases some of the medication particles. Subsequently, the chain of magnetic particles fragments, completely destroying the container. The medication delivery is completed 90 ns after the onset of the magnetic field, accompanied by a complete collapse of the membrane.

4. Conclusions

We applied quaternion molecular dynamics simulations to describe field-induced structural transitions in systems of few magnetic dipoles and their use for targeted medication delivery. We found it possible to contain compact ring isomers of magnetic particles, together with molecules of an active medication, inside inert microcapsules. The filled microcapsules could be transported within the body using a weak, inhomogeneous magnetic field. Our results suggest that a structural transition within the magnetic subsystem, induced by an externally applied strong magnetic field, may be used to rupture a flexible container and to release the active medication. Our studies of six ferromagnetic particles in a hard sphere, modelling a medication microcapsule, indicated that planned delivery can be initiated by applying an external field of 1500 Oe and completed within 100 ns. Accidental release induced by thermal and magnetic fluctuations can be safely avoided under relevant conditions.

Acknowledgments

We acknowledge the assistance of Seong Gon Kim and Philippe Jund in developing the quaternion molecular dynamics code and discussing the application of magnetic systems in medication delivery. We also acknowledge useful discussions with Eberhard Hilf and Heinrich Stamerjohanns, as well as computational support by Andrew Kaminski in the early stages of this study. Partial financial support has been provided by NSF NIRT grants DMR-0103587, ECS-0506309, the NSF NSEC grant EEC-425826, and the Humboldt Foundation.

References

[1] Zhang H and Widom M 1994 *Phys. Rev.* E **49** R3591
[2] Zhang H and Widom M 1993 *J. Magn. Magn. Mater.* **122** 119
[3] Wang H, Zhu Y, Boyd C, Luo W, Cebers A and Rosensweig R E 1994 *Phys. Rev. Lett.* **72** 1929
[4] Jund P, Kim S G, Tománek D and Hetherington J 1995 *Phys. Rev. Lett.* **74** 3049
[5] Raj K, Moshowitz B and Casciari R 1995 *J. Magn. Magn. Mater.* **149** 174
[6] Dickstein A J, Erramilli S, Goldstein R E, Jackson D P and Langer S A 1993 *Science* **261** 1012
[7] Hong C Y, Jang I J, Horng H E, Hsu C J, Yao Y D and Yang H C 1997 *J. Appl. Phys.* **81** 4275
[8] Weis J J and Levesque D 1993 *Phys. Rev.* E **48** 3728
[9] Levesque D and Weis J J 1994 *Phys. Rev.* E **49** 5131
[10] Clarke A S and Patey G N 1994 *J. Chem. Phys.* **100** 2213
[11] Lavender H B, Iyer K A and Singer S J 1994 *J. Chem. Phys.* **101** 7856
[12] Halsey T C and Toor W 1990 *Phys. Rev. Lett.* **65** 2820

[9] The morphology of magnetic particle aggregates, used to transport the medication, is preserved up to a temperature of $T \approx 400$ K. Therefore, the drug delivery mechanism demonstrated at 300 K, shown in figure 4, remains unchanged at the temperature of the human body, even up to 400 K.

[13] Halsey T C, Martin J E and Adolf D 1992 *Phys. Rev. Lett.* **68** 1519
[14] Halsey T C 1993 *Phys. Rev.* E **48** R673
[15] Tao R and Sun J M 1991 *Phys. Rev. Lett.* **67** 398
[16] Borrmann P, Stamerjohanns H, Hilf E, Jund P, Kim S G and Tománek D 1999 *J. Chem. Phys.* **111** 10689
[17] Borrmann P, Jund P, Kim S G and Tomanek D 1996 *Pending patent application* DE19606804 Deutsches Patentamt, Munich
[18] Lipowsky I R and Sackmann E (ed) 1995 *Structure and Dynamics of Membranes* (*Handbook of Biological Physics* vol 1) (Amsterdam: Elsevier)
[19] Jackson J D 1975 *Classical Electrodynamics* 2nd edn (New York: Wiley)
[20] Yoon M and Tománek D 2007 in preparation
[21] Goldstein H 1980 *Classical Mechanics* 2nd edn (London: Addison-Wesley) p 156
[22] Tománek D, Kim S G, Jund P, Borrmann P, Stamerjohanns H and Hilf E R 1997 *Z. Phys.* D **40** 539
[23] Hardy K 1997 *Non-Ionizing Radiation: An Overview of the Physics and Biology* ed K Hardy, M L Meltz and R Glickman (Madison: Medical Physics Publishing) p 268
[24] Nosé S 1984 *Mol. Phys.* **52** 255
[25] Hoover W G 1985 *Phys. Rev.* A **31** 1695